Urban surfaces studied by VIS/NIR imaging from UAV – possibilities and limitations

I. Burud*[a], M. Vukovic[a], T. Thiis[a] and N. Gaitani[b]

[a] Norwegian University of Life Sciences, Faculty of Sciences and Technology, P.O Box 2003, 1433 Ås, Norway;

[b] Norwegian University of Science and Technology, Department of Architecture and Technology, Gløshaugen, Alfred Getz vei 3, NO-7491 Trondheim, Norway,

ABSTRACT

The present research approach aims at analyzing the relation between material properties and their thermal behavior using airborne multispectral imaging in VIS/NIR and IR with sensors mounted on Unmanned Aerial Vehicle (UAV). As a follow up to a pilot study from spring 2016, a survey including several flights spanned over three days, from early morning before sunrise until late evening after sunset, was carried out in Athens in June 2017. The camera specifications for the survey in 2017 were different than the ones used in 2016. The performance of the cameras was evaluated, taking into account atmospheric correction. The images have been combined to form maps of surface temperature distribution and material physical properties. The VIS/NIR images were used to classify the different surface materials, to compute a map of estimated albedo, and to construct a 3D-model of the area. By combining thermal maps with material classification, albedo information and local weather data, thermal material properties could be characterized for the various materials. The derived properties from this dataset yield valuable information for improved simulation models of urban climate.

Keywords: UAV, Thermal imaging, Multispectral imaging, Material properties, Thermal inertia

1. INTRODUCTION

In the field of urban climatology, special emphasis is given to the surface temperature of urban materials. The surface temperature modulates the temperature of the lowest atmospheric layers and is central to the surface energy balance and the human thermal comfort. Furthermore, this has a significant contribution to the phenomenon of the urban heat island (UHI) e.g. "modified thermal climate that is warmer than the surrounding non-urbanized areas, particularly at night" [1, 2]. The thermal inertia (TI) ($J\ m^{-2}K^{-1}\ s^{-1/2}$) of a material is a measure of its responsiveness to variations in temperature. It is one of the typical parameters for describing the thermal characteristics of subsurface materials and is defined as

$$TI = \sqrt{\rho c k} \tag{1}$$

where k is the thermal conductivity (W $m^{-1}K^{-1}$), ρ the bulk density (kg m^{-3}), and c the specific heat (J $kg^{-1}K^{-1}$) of the bulk soil material. Materials with a high heat capacity display high thermal inertia. Consequently such materials will show small changes in temperature through the diurnal cycle [3].

According to studies [4], higher thermal inertia is observed in urban areas than that of rural areas. However, remote estimates of urban thermal inertia show anisotropy effects due to thermal anisotropy [5].

In remote sensing TI is measured by diurnal changes in temperature. Apparent thermal inertia (ATI) gives a quantification of the effect of thermal inertia on surface temperature based on remotely sensed observations [6]. ATI have been computed from remote sensing measurements of the diurnal temperature amplitude (DTA), the albedo (α), and the incoming solar radiation [7]. This approach was also applied in a similar UAV survey in 2016 [8,9].

In traditional satellite imagery the spatial resolution and the time sampling rate are usually limited. Aerial survey using UAVs makes it possible to obtain high resolution geo-referenced thermal and visible/NIR maps of an area at flexible time intervals. A survey using UAV in Athens, Greece, is presented here in order to study thermal properties for urban surfaces in a particular suburb of Athens where measures have been taken in order to reduce the urban heat island effect.

In order to understand and mitigate UHI, it is a goal to accurately predict and simulate the urban microclimate. There are numerous simulation models developed for this purpose [10, 11, 12]. One particularly promising model is the SOLWEIG model [11] which utilizes a geographical information system (GIS) and is particularly computationally inexpensive due to efficient parameterization of the surface temperature of several urban materials. A linear relationship between maximum solar elevation and maximum difference between surface temperature, T_s, and air temperature, T_a, under clear sky conditions was used to estimate surface temperature, as

$$T_s - T_a = a * (maximum\ solar\ elevation) - b \quad (2)$$

where a and b are constants specific for each material. The following analysis is inspired by the SOLWEIG model and aims at improving future model simulations by improving the material parameters related to their thermal properties.

2. MATERIALS AND METHODS

2.1 Data acquisition

UAV measurements were carried out on June 2017 at the Municipality of Ymittos which is a suburb, situated 2.5 km southeast from the center of Athens, Greece, as a follow up to the survey carried out in 2016 [8,9]. An aerial RGB image from the survey is shown in Fig. 2. The study area is subject to the urban heat island effect, and several measures have been taken by the municipality to diminish the local temperature, such as using cool materials (cool coating on asphalt, marble) and by incorporating water, vegetation and solar shading devices.

Images from the UAV were obtained in the visible, NIR and IR part of the electromagnetic spectrum. The UAV used in the survey was a DJI Phantom 4 with a factory installed RGB camera with a GPS included. In addition to the RGB camera a rebuilt RGB camera where the blue channel is replaced by a NIR channel (Canon SX280 rebuild by Maxmax.com) was mounted on the UAV in order to obtain NIR images of the area. This camera also has an included GPS logger. Thermal (IR) images were obtained by mounting a radiometric IR camera (FLIR Vue Pro) with a 9mm lens on the UAV.

The pixel size of the pictures varied from 8-80 mm depending on the type of sensor. The flights were programmed to follow a predetermined route at an altitude of 100 meters and the cameras were set up to record every other second. A standardized grey calibration plate reflecting 60% of the solar radiation was recorded before and after each set of VIS/NIR images in order to calibrate for varying light conditions between the flights. In situ images of the different materials were also recorded with an RGB camera, an IR camera and the VIS/NIR camera.

In order to check for the influence of the atmosphere from the ground up to 100 m, measurements were carried out with the UAV centered on one geographical spot, lifting from 0 to 100 m and pausing approximately every 5 m, recording measurements. In addition, the radiometric accuracy of the thermal camera (FLIR vue pro R) was compared to the one used in the 2016 survey (Optris PI 640) by simultaneously recording the signal from materials with different temperatures in a laboratory environment. Weather data were obtained from a local weather station. In addition, in-situ measurements were conducted of air temperature and relative humidity (with shielded sensors) and of solar radiation (pyranometer).

The weather on June 18th, the day before the survey start had heavy rain, rather unusual for the season, as can be seen in Fig. 1 where precipitation and temperature are displayed from June 15th t June 22th. The soil and vegetation and some of the asphalt were therefore still moist at the start of the survey. On June 19th there was no precipitation but there were some clouds around noon. June 20th was a clear and sunny day, and June 21th was warm with a thin layer of clouds.

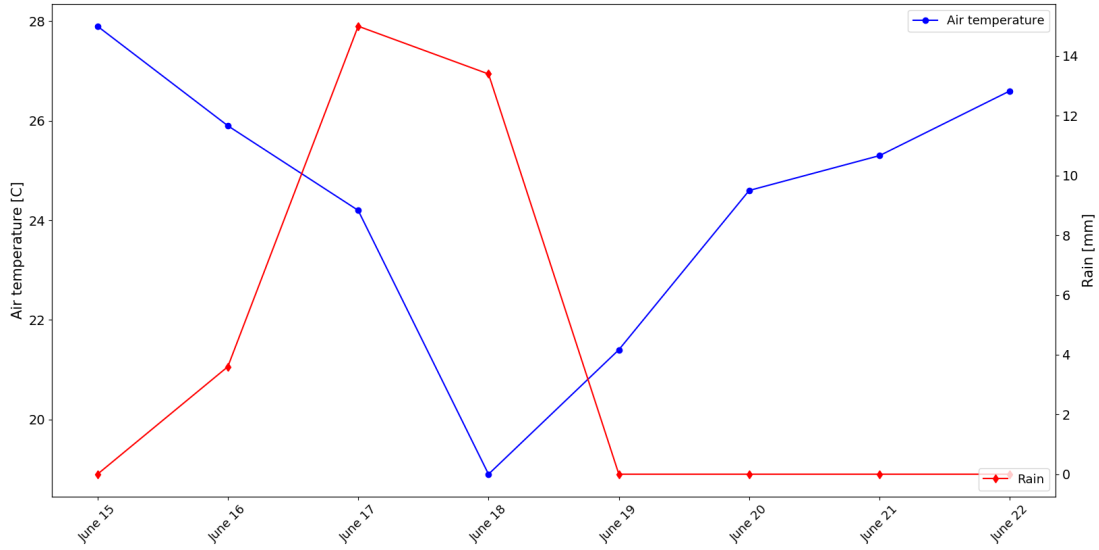

Fig 1. Daily mean values of temperature and precipitation in Athens from June 15th to June 22th 2017.

2.2 Data analysis and methodology

The RGB, VIS/NIR and IR images obtained with the UAV were combined and corrected for geometric distortions (orthorectification process) [13] using the software Pix4d [14]. From the RGB images a digital surface model (DSM) of the area was computed. GPS coordinates from the RGB camera were used to georeference the IR images. This was done by synchronizing time stamps from the two data sets using Exiftool [15]). The RGB, NIR and thermal maps were finally aligned to the detailed map of the buildings in the area provided by OpenStreetMap (openstreetmap.org) by manually selecting corresponding reference points using QGIS. This resulted in a stack of aligned images of all the observed wavelengths.

The stack of RGB, NIR and Normalized Differential Vegetation Index (NDVI) images was used to classify the various surface materials in the area. The algorithm for the computation of NDVI is given by equation (3):

$$NDVI = \frac{NIR-R}{NIR+R} \tag{3}$$

where NIR and R are reflectance values in the near infrared and red parts of the electromagnetic spectrum respectively. A supervised Maximum Likelihood classification was applied using Semi-Automatic Classification Plugin (SCP) from the open-source system QGIS. The classification was carried out based on region growing algorithm as an image segmentation method. This implies that pixels with spectral distance below a certain threshold value were selected as a region of interest [16].

The IR measurements as a function of height at the same spot indicated that the atmosphere had an influence of approximately 10% of the temperature value at 100 m. This complies well with theory [17] that has been implemented into the python function raw2temp that computes temperature from raw IR frames for various heights and weather conditions (humidity, air temperature) [18]. This effect should therefore be taken into account when studying absolute temperatures with a high accuracy camera. The analysis of the laboratory study of the two IR cameras (Optris and FLIR) showed that the Optris camera had a systematic error of 0.5 degrees and a fluctuation of 0.1 degrees whereas the FLIR camera had an offset error of 3 degrees and fluctuations of 0.5 degrees. These offsets and fluctuations are within the

stated errors from the camera producers. Given the high uncertainty of the FLIR camera it was concluded that the atmospheric effect was negligible compared to the overall accuracy of the FLIR camera in the 2017 survey.

The IR radiation emitted by a material depends not only on its temperature but also on the emissivity of the measured object. In order to obtain calibrated temperature values from the IR images, the emissivity of each surface material across the imaged area must therefore be taken into account. The classification of the RGB and NIR images was used to assign emissivity values to the thermal maps. Four classes of emissivity materials were selected from the literature [19]: water, asphalt, soil and vegetation and assigned to the surface materials classified with the Maximum Likelihood Classification algorithm.

In total nine surface temperature maps were obtained from early morning before sunrise on June 19th to noon on June 21th. The difference between the temperature obtained at 13:30 (maximum temperature) and the one from 05:30 (minimum temperature) was computed as the DTA on June 19th and 20th, and these were used to compute the ATI for these days.

The ATI was calculated using the equation [17]:

$$ATI = S * \frac{(1-\alpha)}{DTA} \quad (4)$$

where S is the solar fraction involving geographical location, local shading and α is the albedo. The albedo image was computed as described in [9] and ATI was computed with S representing the fraction of solar radiation relative to an area with no shadow.

The times series of temperature maps were also used to explore the thermal properties of the materials in the area. By combining the temporal distribution of the surface temperature of the different materials with the measured solar radiation revealed how fast the materials heat up and cool down relative to the daily solar elevation cycle. This is an indicator on the responsiveness of the materials to adapt to the surrounding temperature, i.e., their thermal inertia. However, this methodological approach requires the study of the non-shaded areas (i.e. the ones that have been exposed to solar radiation during the whole day). The digital surface model (DSM) combined with solar declination and geographical location were used to map the shadows in the area throughout the day, using the UMEP plugin as a part of QGIS [20]. This shadow map was then used to select unshaded regions to compute the temperature time series for the following materials: asphalt, concrete, marble, vegetation, water and soil. The classification of the materials described above was used to select the regions for each material. The maps of shadows with a sampling of once per hour through the day were also used to compute the cumulative daily solar radiation map for the area. In the shaded areas, only the diffuse solar radiation was included in the daily radiation map. Since the measured solar radiation was limited to the global horizontal radiation, the diffuse radiation was estimated by [21]

3. RESULTS AND DISCUSSION

3.1 Classification of materials

A section of the RGB image and the classification of the materials performed on the stack of RGB, NIR and NDVI are shown in Fig. 2. A total of 10 different classes were selected for a Maximum Likelihood Classification. Classes of asphalt, marble, soil, grass, trees, water, solar cells and roofs were chosen. Note that two different classes could be distinguished for the asphalt, which corresponds to color differences and different coatings of the asphalt. The asphalt marked as dark grey in Fig. 2b) has been covered with “cool coating”, and the coating seems to be worn due to cars and weathering. There are therefore streets with an apparent mix of the two types of asphalt.

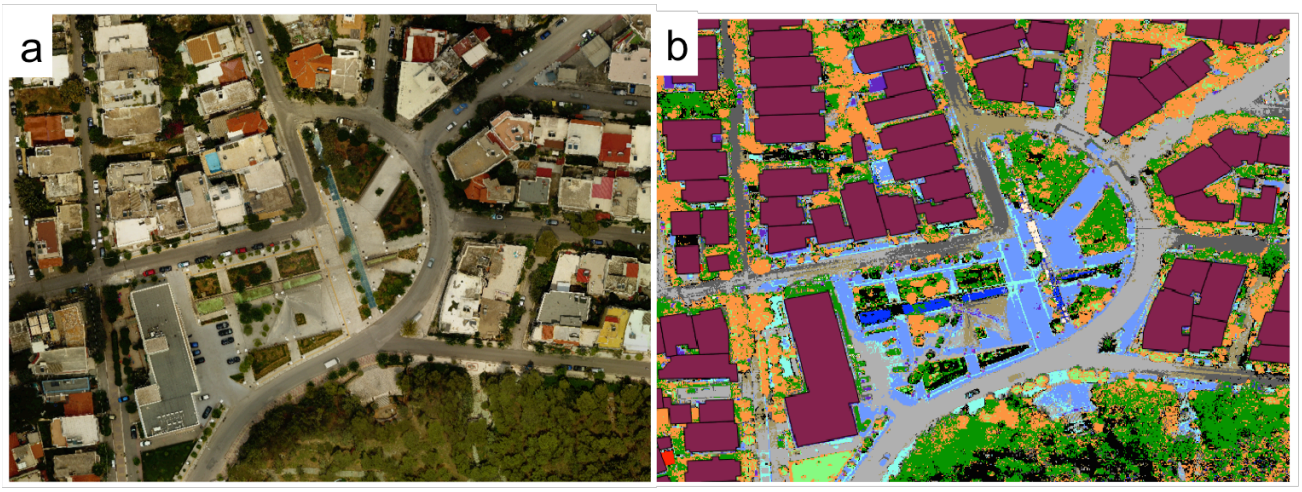

Fig 2. a) RGB image of the survey area in Athens, b) Classification of the surface materials of the area: green and orange = trees and bushes, black = soil, light green = grass, light blue = marble, dark blue =water, grey (dark and light) =asphalt, turquoise = tiles for blind, dark red = roofs.

A map of the solar radiation in each pixel from sunrise until 17:00 is shown in Fig. 3a), using the model based on the sun elevation and the 3D-model described above, the in-situ measurements of global horizontal radiation and the estimation of diffuse radiation by [21]. The derived albedo map from the calibrated RGB and NIR reflectance bands is shown in Fig. 3b).

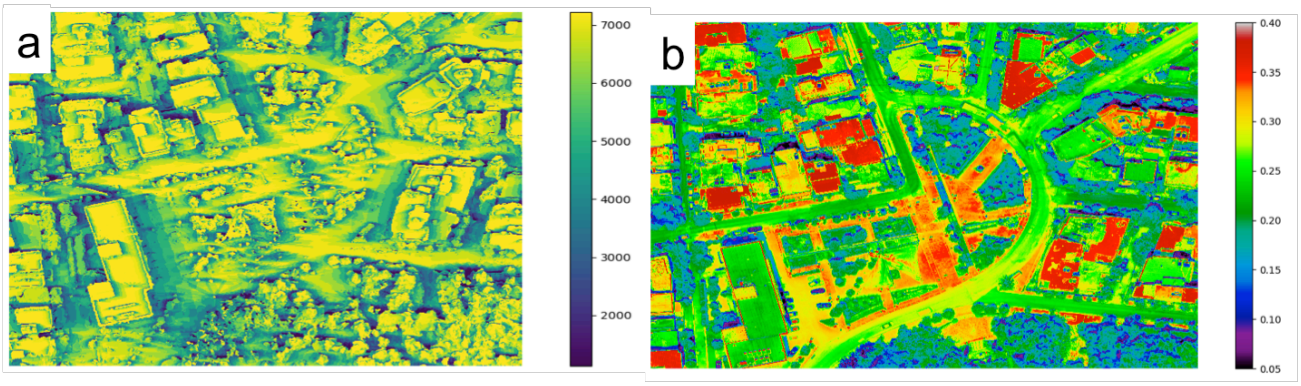

Fig 3. a) Map of cumulative daily solar radiation in (W h m^{-2}) on June 20th 2017; b) Albedo map derived from calibrated RGB and NIR reflectance maps.

3.2 Temperature maps

From the derived temperature maps the diurnal temperature amplitude (DTA) was computed from the maximum and minimum surface temperature observations The DTA maps obtained from June 19th and 20th 2017 are shown together with the one from April 12th 2016 [8,9] in Fig. 4. The DTA distribution on June 20th presents the highest values and the one from June 19th has considerably lower values, e.g. the DTA values of the asphalt ranges between approximately 15 to 20 degrees on the 19th, whereas the values on June 20th vary between 25 and 35°C. For the April 12th 2016 the DTA values vary from 25 to 35°C, hence very similar to the ones from June 20th 2017. This corresponds well with the weather data from the three days, i.e. some clouds in the middle of the day on June 19th, whereas a clear and sunny day on the 20th and April 12th. All three maps also indicate that the asphalt has the highest temperature difference of all the materials, between 30 and 40 degrees as indicated on the map from June 20th 2017. The variation of DTA of marble is smaller than asphalt as shown consistently on all three maps. Again on June 20th 2017 the difference in marble's temperature was the

highest, around 28 degrees. Also all three maps suggest that the temperature difference in the park (lower part of the images) is among the lowest in the area with a temperature difference in the park of approximately 15 degrees in Fig. 4 a) and b) while the maximum temperature difference for vegetation seems to be around 20 degrees in Fig. 4 c). This indicates that the diurnal variation in temperature in the areas with vegetation is considerably smaller than the variation in the temperature of asphalt and marble.

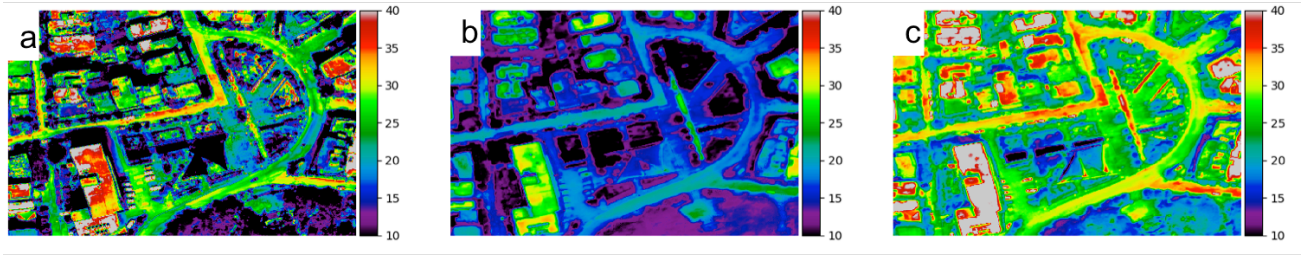

Fig 4. Diurnal temperature amplitude maps, difference between maximum and minimum temperature (in °C) of the day from a) April 12th 2016, b) June 19th 2017 and c) June 20th 2017.

The DTA observations coincide well with maps of ATI weighted with solar radiation, as shown in Fig. 5. The ATI values seem to be higher for the map from June 19th 2017 compared to the map from June 20th 2017 and April 12th 2016. The reason for that can be found in the DTA-maps in Fig. 4 in connection with equation (3). The temperature difference on these two days was higher and thus the ATI-maps have lower values. Looking at each map separately it can be observed that the highest values of ATI, 0.08 K^{-1} and above, are displayed in the areas with the lowest temperature differences such as vegetation and water. ATI values for asphalt and marble, however, appear to be the same on both maps even though there is visible difference in their variation in temperature as mentioned above. A reason for that could be that marble has higher albedo values, above 0.30, while asphalt has lower albedo values, slightly above 0.20, also reported in [9]. Marble also has the highest thermal conductivity compared to the other examined materials (asphalt, concrete, and vegetation). It should also be noted that there was heavy precipitation on June 18th and the soil was still moist at the beginning of the survey on June 19th. This can be seen in the areas with bare soil (see Fig. 1) on the ATI images, since these areas have very different values between June 19th, where the soil was still moist, and June 20th where it had dried. This difference is not as apparent in the park in the lower part of the image since the temperatures recorded here is mainly the temperatures of the three tops

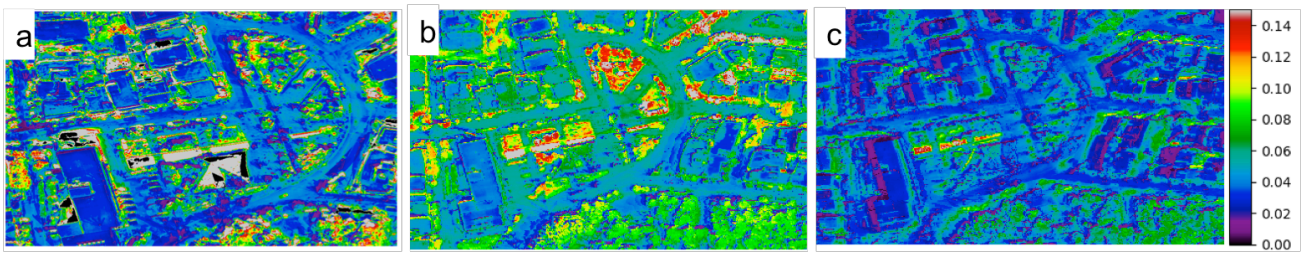

Fig 5. Apparent thermal inertia (ATI) weighted with the solar radiation for each pixel, from a) April 12th 2016, b) June 19th 2017 and c) June 20th 2017.

3.3 Temperature time series

As an alternative to maps of ATI, the thermal properties of the materials can be derived from the time series of the temperature maps. The average temperature for different materials in regions with areas with little or no shade during the day over is plotted with time in Fig. 6. Note however that at 17:00 some of the areas of soil, tiles and concrete had been in shade for a few hours, hence introducing larger uncertainties for these points. The solar radiation measured at the site is also plotted with a time sampling of one hour. It can be seen that the materials with low thermal inertia, or ATI (see Fig. 5) have steeper curves and higher amplitude than the materials with high ATI.

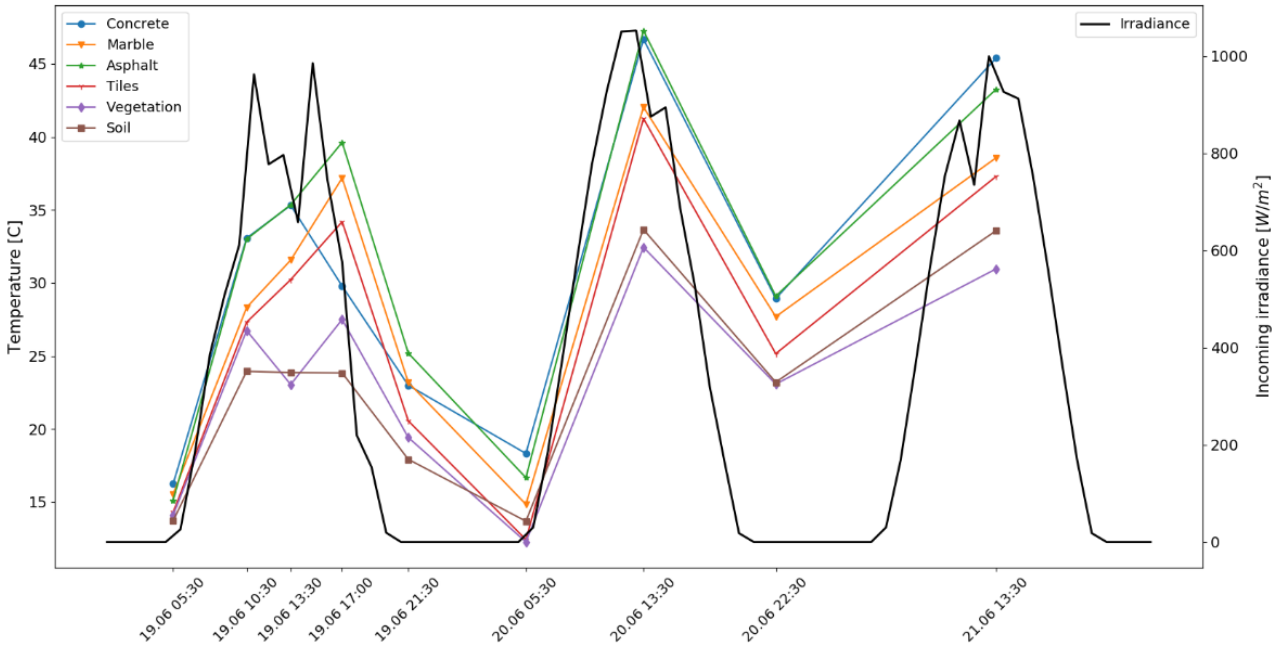

Fig 6. Temperature curves of different materials from early morning on June 19th until noon June 21th. Also plotted in solid black is the solar radiation.

Based on the measured temperatures and the solar angle in Athens derived from [21] the simple parameterization approach proposed in [11] could be adopted. Fig. 7 shows the simple parameterization of asphalt, marble and vegetation. The curves display a sinusoidal curve where the phase and amplitude are determined from the measurements and the measurement points overlaid. Each of the three curves then represents a linear relation between the maximum solar elevation during the day and the maximum difference T_s - T_{air} as described in Eq. 1. It can be seen that the measurement points are lower than the modeled ones for all three materials, and the difference is higher than the error uncertainties on the measurements. There are several reasons for these differences. Firstly, the maximum temperature of the day was not really measured since flights were only performed at 13:30 and 17:00. Secondly, the weather was cloudy on June 19th and followed a heavy rainfall and the measurements are therefore not really suited for this model, since it is required that the measurements must be undertaken in a clear and dry day [11]. Thirdly, there are big variations within each material. There are for examples at least two types of asphalt in the area. And finally, the materials are subject to weathering, which might change the albedo. The albedo of the material is not taken into account in this simple parameterization model.

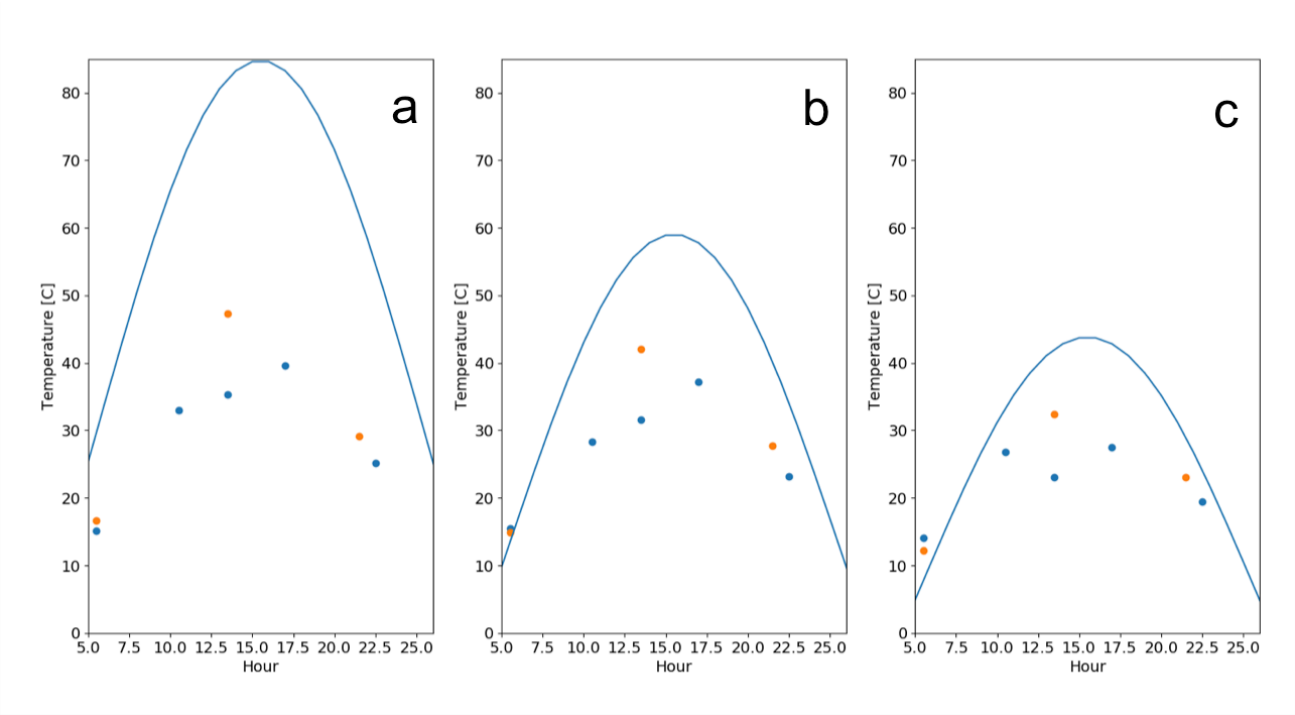

Fig 7. Sinusoidal modeling of temperature using the simple parameterization model from [9] with measurements from June 19th (blue) and June 20th (orange).

4 CONCLUSION

Due to the strong heterogeneity of surface characteristics, the surface temperature varies in space as well as in time and an adequate characterization requires measurements with detailed spatial and temporal sampling. UAV survey provides potential for very high resolution mapping at a user-defined frequency. The results confirm that aerial survey of urban materials is well suited approach for classifying materials at the urban fabric and providing information about their physical properties.

The thermal properties seem to be well modeled with the ATI derived from the measurements. The ATI weighted with incoming solar radiation is a good indicator of the surface temperature during the daily cycle for dry materials. For moist materials such as soil and vegetation the relation is different which need to be taken into account when modeling the surface temperature.

For the simple parameterization of the thermal properties based on solar angle and maximum temperature difference, there appeared to be four main limitations: 1) the radiometric accuracy of the thermal camera and 2) the variations in the local weather conditions, 3) the variations within the materials and 4) influence of albedo.

Future studies are planned where the parameterization model from [11] is applied on the measurements used as input for numerical simulations of the surface temperature of the materials.

REFERENCES

[1] Landsberg H.E. (1981) The Urban Heat Island, Academic Press NY

[2] Voogt, J.A, Oke, T.R., "Thermal remote sensing of urban climates," Remote Sensing of Environment 83, 370-384 (2003)

[3] M. Sohrabinia et al, “Soil moisture derived using two apparent thermal inertia functions over Canterbury, New Zealand”, J. Appl. Remote Sens. 8(1), 083624 (doi:10.1117/1.JRS.8.083624) (2014)

[4] Berwal, S., Kumar, D., Singh, V.P., Pandey, A.K., Kumar, K., "Dynamics of thermal inertia over highly urban city: A case study of Dehli", Proceedings of SPIE, 1008, pp7 (2016)

[5] Zhan, W., Chen, Y., Voogt, J. A., Zhou, J., Wang, J., Ma, W., Liu W. "Assessment of thermal anisotropy on remote estimation of urban thermal inertia", Remote Sensing of Environment 123, 12-24 (2012).

[6] Y.Qin, "Pavement surface maximum temperature increases linearly with solar absorption and reciprocal thermal inertia", International Journal of Heat and Mass Transfer 97, 391-399, (2016)

[7] Van doninck, J. et al, "The potential of multitemporal Aqua and Terra MODIS apparent thermal inertia as a soil moisture indicator," International Journal of Applied Earth Observation and Geoinformation 13, 934-941 (2011).

[8] Burud, I., Thiis, T., Gaitani, N., "Reflectance and thermal properties of the urban fabric studied with aerial spectral imaging" SPIE Proceedings Vol. 10444, Fifth International Conference on Remote Sensing and Geoinformation of the Environment (2017)

[9] Gaitani, N., Burud, I., Thiis T., Santamouris, M., "High-resolution spectral mapping of urban thermal properties with Unmanned Aerial Vehicles." BUILDING & ENVIRONMENT (available online: https://doi.org/10.1016/j.buildenv.2017.05.027 (2017)

[10] Bogren, J., Gustavsson, T., Karlsson, M., Postgård, U. "The impact of screening on road surface temperature." Meteorol Appl 7:97-104 (2004)

[11] Lindberg, F., Holmer, B., Thorsson, S., "SOLWEIG 1.0 – modeling spatial variations of 3D radiant fluxes and mean radiant temperature in complex urban settings. Int. Biometeorol 52:697-713, (2008)

[12] Lindberg, F., Onomura, S., Grimmond, C.S.B. "Influence of ground surface characteristics on the mean radiant temperature in uban areas." Int J Biometeorol 60(9):1439-52, (2016)

[13] M. Jaud, et al. "Method for orthorectification of terrestrial radar maps." ISPRS Journal of Photogrammetry and Remote Sensing 97, 185-194 (2014)

[14] (http://owl.phy.queensu.ca/~phil/exiftool/

[15] Congedo, L., "Basic tutorial 1: Land Cover Classification of Landsat Images," <https://fromgistors.blogspot.com/2018/02/basic-tutorial-1.html> (2018)

[16] PIX4d Software: https://pix4d.com/ Accessed on

[17] Minkina, W. and Dudzik, S. 2009. Infrared Thermography: Errors and Uncertainties. Wiley Press, 192 pp. (2009)

[18] https://www.rdocumentation.org/packages/Thermimage/versions/2.2.3/topics/raw2temp

[19] Oltra-Carrio, R. Sobrino, J. A., Franch, B., Nerry, F., «Land surface emivissivity retrieval from airborne sensor over urban areas». Remote Sens. Of Environment, 123, 298-305,(2012)

[20] http://urban-climate.net/umep/UMEP_Manual

[21] Bird, R. E., and R. L. Hulstrom, *Simplified Clear Sky Model for Direct and Diffuse Insolation on Horizontal Surfaces*, Technical Report No. SERI/TR-642-761, Golden, CO: Solar Energy Research Institute, (1981)